Renewable Energy 206 (2023) 1198–1211

Contents lists available at ScienceDirect

Renewable Energy

journal homepage: www.elsevier.com/locate/renene

Characterising the wave energy resource of Lanzarote, Canary Islands

David Christie [a,*], Simon P. Neill [a], Peter Arnold [b]

[a] School of Ocean Sciences, Bangor University, Menai Bridge, LL59 5AB, Wales, UK
[b] Bombora Wave Power, The Offices, Cleddau Reach, Pembroke Dock, SA72 6UJ, Wales, UK

ARTICLE INFO

Keywords:
Wave energy
Spectral modelling
Simulating waves nearshore SWAN model
Resource assessment
Wind-wave co-location
Metamodel

ABSTRACT

Waves of varying magnitude and frequency, characteristic of all coastal locations throughout the world, could be converted into electricity via wave energy converters. However, one challenge with wave energy conversion is lack of knowledge of the regional distribution of wave properties (e.g. to optimise site selection), and how the wave power varies at inter- and intra-annual timescales. Here, we apply physics- and non-physics-based approaches to accurately simulate the wave climate of the Canary Islands—a region in the eastern North Atlantic that relies heavily on the import of diesel to generate much of its electricity. Over the 11-year time period of the physics-based wave hindcast, the annual mean wave power of Lanzarote, one of the largest of the Canary Islands was approximately 25 kW/m along the exposed north-western coast of the island. We find that intra-annual variability was relatively low (compared with high latitude regions such as the west coast of Scotland), with the coefficient of variation for wave energy resource = 1.1. To reduce levelized cost, it could be advantageous to co-locate wave energy arrays with mature offshore wind energy, and we find that the dominance of swell waves in Lanzarote reduces the coefficient of variation for a 55% wind, 45% wave combination to 0.8. Finally, we demonstrate a simple non-physics based process for extending the output timeseries beyond the hindcast duration, by correlating with parameters from global models.

1. Introduction

With continental coastlines exposed to high energy densities generated by thousands of kilometres of fetch, the theoretical annual global wave power potential has been estimated at 29,500 TWh, sufficient to meet the world's annual electricity demand, which was 22,900 TWh in 2019 [1–3]. Creating a strong wave energy sector to tap into this potential will support global efforts to address climate change (and energy insecurity) by contributing to a robust and diverse renewable energy mix. Expansion in installed wave energy capacity is urgently needed to improve grid resilience and decarbonise island communities.

The wave energy industry benefits from and is impaired by its diversity of technology. There is an ecosystem of different types of device, optimised for different water depths and wave characteristics. However, this poses practical challenges: each device requires its own trajectory of development and in situ prototype and array-scale testing. A heterogeneous global network of consented (and, ideally, grid-connected) test sites is crucial. One such site is the Atlantic island of Lanzarote, which lies about 1000 km from the Iberian Peninsula and 125 km from the African coast.

1.1. Modelling Lanzarote's wave resource

Lanzarote, located between latitude 28°14′N and 28°49′N and longitude 7°13′W and 7°14′W, is the fourth largest of the Canary Islands (Fig. 1)—a Spanish autonomous community in the Atlantic Ocean. Including islets, it has an area of 846 km^2, and runs 60 km north-south, and 20 km east–west. The northern coast, in particular, is an attractive location for wave energy extraction. Direct exposure to Atlantic swells results in a potentially large and relatively consistent energy resource.

General information about a location's suitability for wave energy extraction may be obtained from analysing the outputs of regional-scale models. For example, Sierra et al. [4], explored wave power at nine data points around Lanzarote, extracted from long-term 0.25° × 0.25° resolution models. Although all the sites were in deep water, considerable spatial variation in power and direction was observed (including at adjoining data points), with the archipelago acting as an obstacle. With each island covered by only one or two grid points (as can be seen in Fig. 1 showing the Canary Islands with a 1° grid overlaid), care should be taken when interpreting these model outputs for wave modulation due to the islands. Furthermore, the grid is too coarse for variation along the coastline itself to be resolved explicitly.

* Corresponding author.
E-mail address: d.christie@bangor.ac.uk (D. Christie).

https://doi.org/10.1016/j.renene.2023.02.126
Received 19 November 2022; Received in revised form 30 January 2023; Accepted 25 February 2023
Available online 25 February 2023

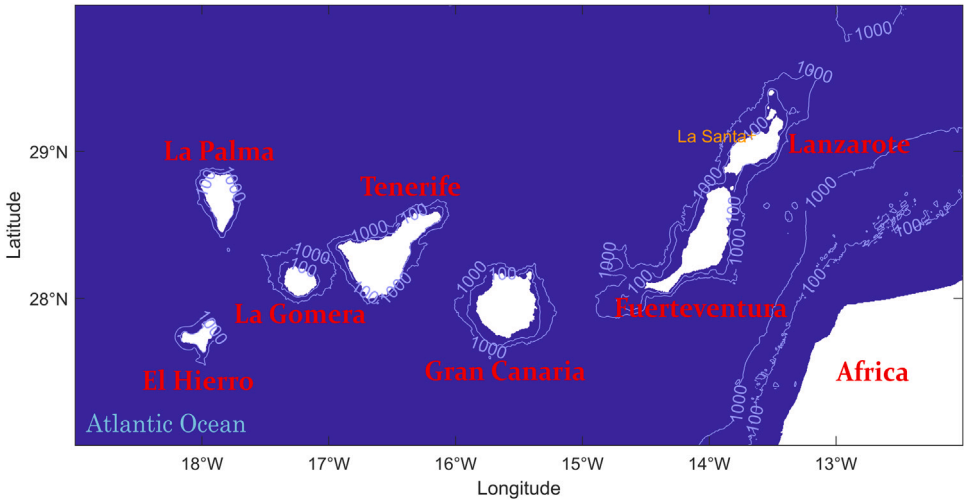

Fig. 1. Map of the Canary Islands, including Lanzarote in the north-east, with the La Santa deployment site labelled. The 100 m and 1000 m bathymetric contours indicate particularly steep gradients in the region: more detailed bathymetry for Lanzarote and the deployment site is shown in Fig. 2.

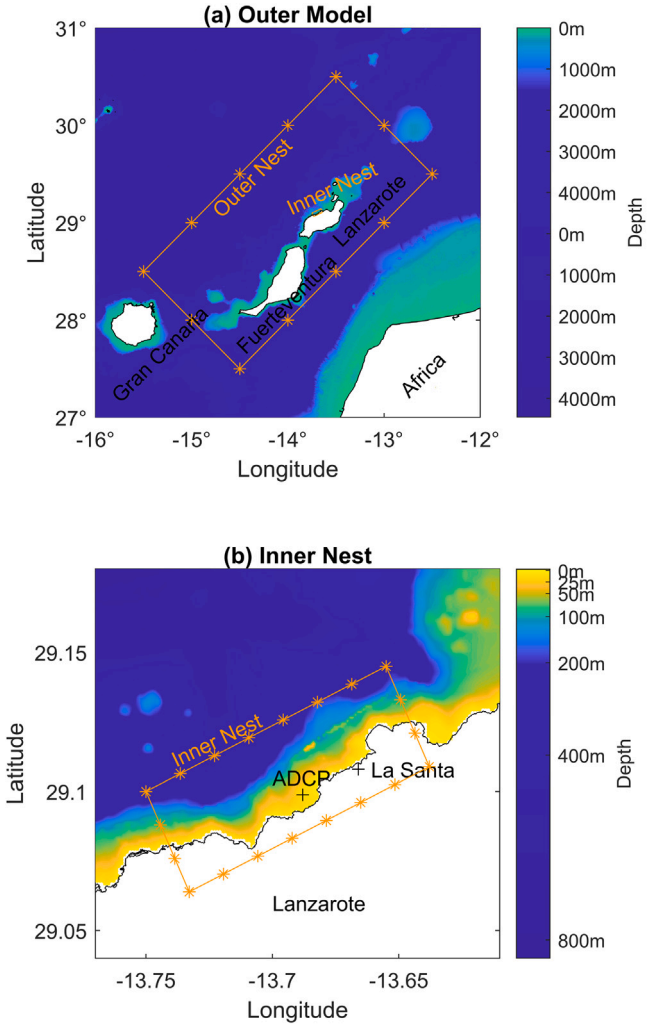

Fig. 2. The two nested SWAN model domains, with the boundaries shown as red boxes. The rapidly varying bathymetry in the Lanzarote coast poses challenges for model construction. The asterisks in (a) correspond to the global ERA-5 spectra available at $0.5° \times 0.5°$ resolution, which act as the (spatially and temporally varying) boundary conditions for the outer model. The asterisks in (a) are the grid points from the outer model (b) constituting the boundary input for the nested inner model.

A similar study for the Canary Island of El Hierro, based again on a North Atlantic wave model with $0.25° \times 0.25°$ resolution, found similar spatial variability, and also explored seasonal dependence [5].

Regional scale models such as those used in [4,5] give a useful overview of the nature of the wave resource in a particular part of the world. However, to identify potential areas for energy extraction, more detail must be obtained on the spatial distribution of wave energy. This requires a higher resolution local simulation, using a spectral wave code such as SWAN [6], often driven at the offshore boundaries by output from a larger regional or global model. One such multi-decadal hindcast model for the entire Canary Islands group (including Lanzarote) was considered by [7], while similar studies have also used SWAN modelling to investigate the wave resource of island groups such as the Azores [8] and the Cape Verde Islands [9].

The Canary Islands are a volcanic archipelago characterised by extremely steep bathymetric gradients. These can lead to large spatial inhomogeneities in nearshore resource, with extremely localised "hotspots" resulting from bathymetric features. The Canary Islands SWAN model [7] used a $0.1° \times 0.05°$ grid, with almost all of the model domain points situated in deep water. To characterise the wave resource available for nearshore energy harvesting (and optimise deployment) one must additionally resolve the rapid local-scale bathymetry-induced variation. This requires a further level of nesting. Such a high-resolution local model was created for Tenerife [10] which characterised two representative seastates, and investigated the effect of wave energy converter placement. A local-scale model for the energetic north coast of Lanzarote has not been hitherto created, and sub-kilometre resolution multi-annual hindcasts have not yet been produced for any of the Canary Islands. These gaps will be addressed in the following.

1.2. Renewable energy in Lanzarote

The Canary Islands represent the global energy situation in microcosm. A move is underway to replace high dependence on fossil fuels (expensive imported diesel) with increasing use of renewables, with an aim of halving fossil fuel use by 2030. Renewable use has rapidly increased from 7.8% in 2017 to 19.9% in 2021 [11], driven by expansion in wind power although an ambition to further diversify the energy mix is supported by infrastructure investment. Proposed connectivity improvements in the weakly-meshed network (for example with submarine links between Lanzarote and the neighbouring island of Fuerteventura) and a significant increased in energy storage (including the Salto de Chira pumped-storage hydroelectric power station on Gran

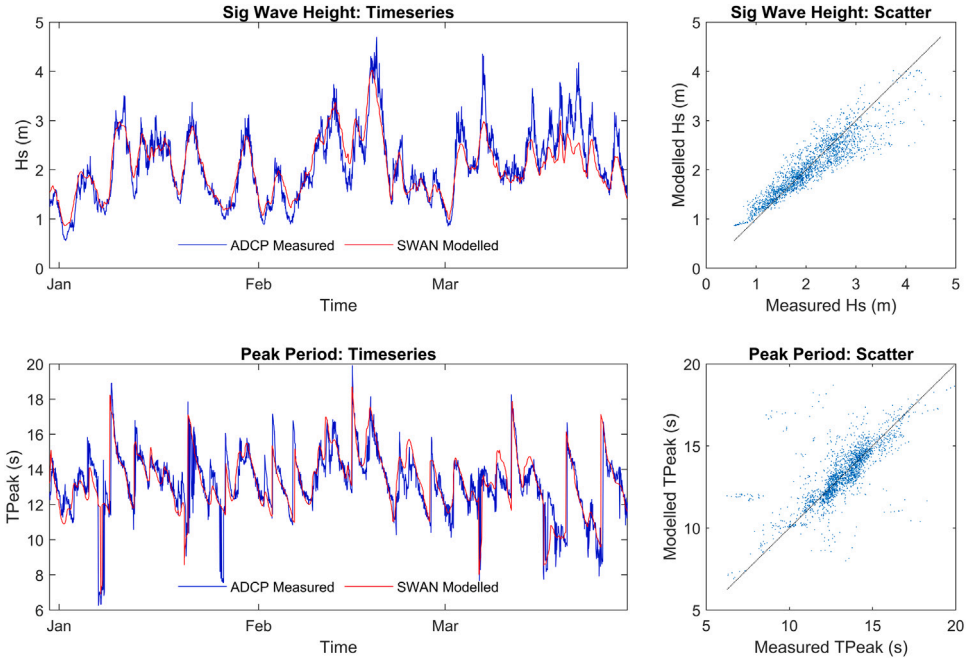

Fig. 3. Timeseries and scatter plots of SWAN-modelled and AWAC-measured H_s and T_p from 30 December 2019–29 March 2020. The SWAN simulation closely tracks the AWAC measurements, although the maxima and minima are sometimes less pronounced.

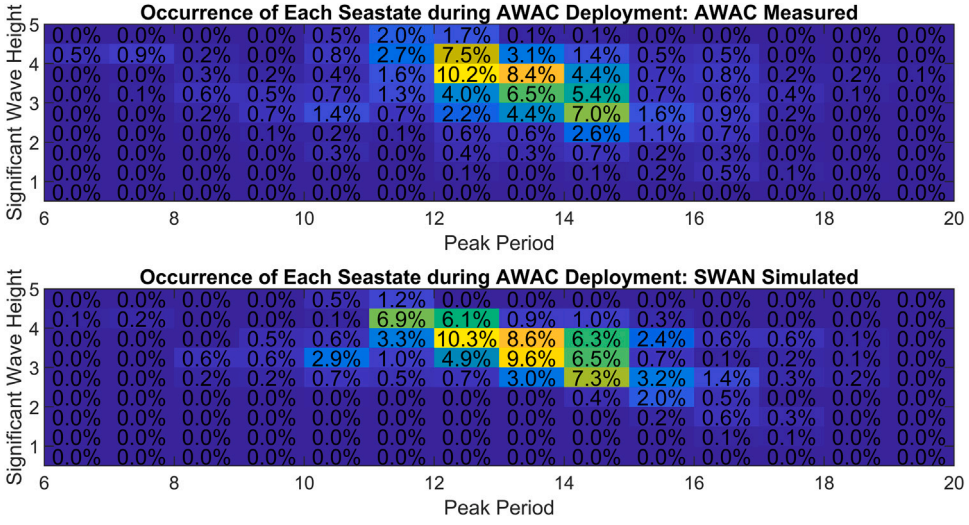

Fig. 4. The occurrence frequency of each $H_s - T_p$ seastate combination, as a percentage of the 2,100 hourly AWAC measurements (top) and 2100 corresponding SWAN calculations (bottom).

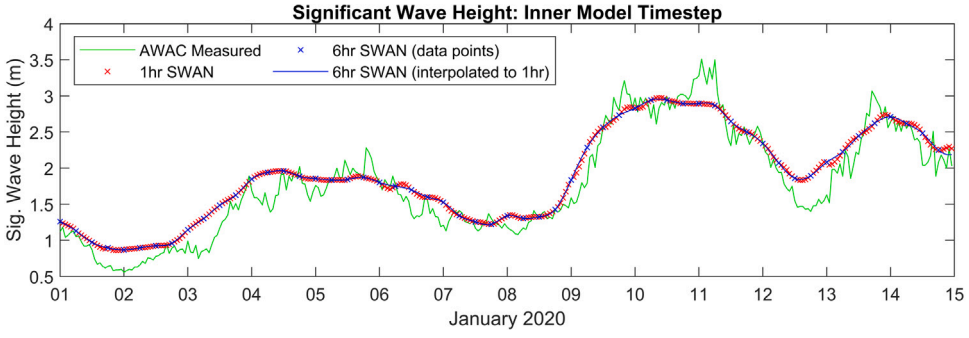

Fig. 5. The inner model run with hourly (red) and interpolated six hourly timestep (blue). A six hourly timestep is sufficient to resolve the model's temporal variation.

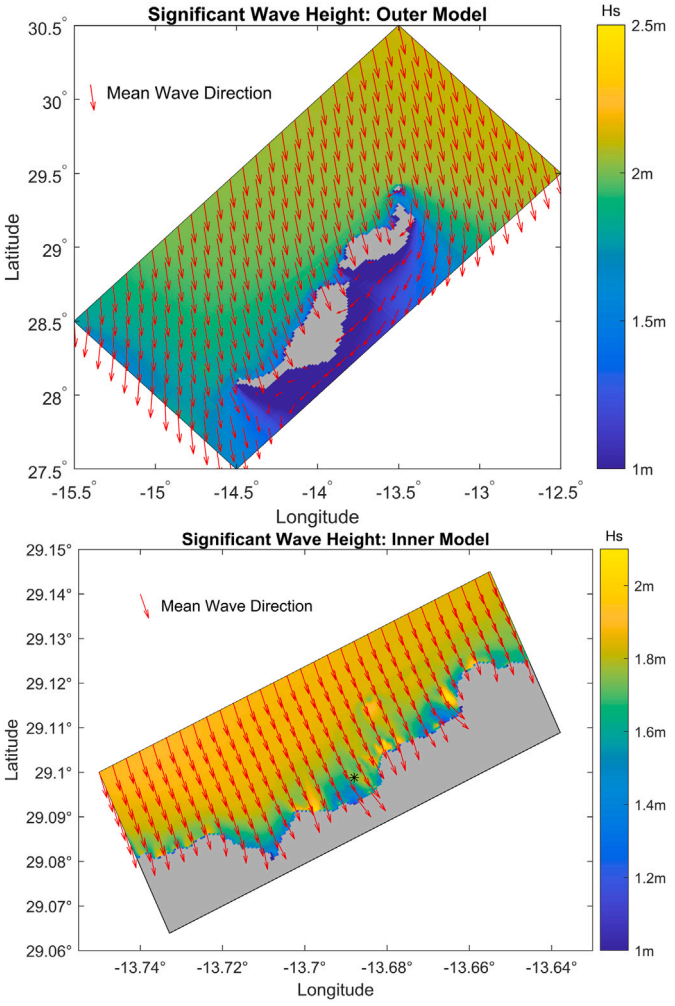

Fig. 6. Eleven year averaged H_s for the outer model (top) and inner model (bottom). Vectors indicate mean wave direction.

Canaria) are projected to lead to significant reductions in renewable energy costs [12].

Bombora Wave Power has been selected to provide up to 4 MW of wave power from a grid-connected site at La Santa, on the north-east of Lanzarote. Electricity will be generated using Bombora's "mWave" membrane style submerged wave energy converters, each of which is rated at 1.5 MW. The submerged membranes pump air through a turbine to produce electrical power: being positioned 10 m beneath the water surface ensures survivability in energetic environments, and removes any visual impact – a key advantage that tidal turbines, for example, have over the majority of wave energy converters [13].

The Bombora device design is also ideally suited for co-location with offshore wind turbines, since it can be attached to the wind turbine substructure itself. Co-locating wave energy devices with offshore wind turbines can reduce energy costs by utilising common grid connections, and exploiting synergies in the consenting process and operation and maintenance procedures. By reducing wave heights at windfarms, maintenance weather windows may also be enlarged [14,15]. Crucially, the variability in output power may be reduced by such a hybrid development — this requires areas of low covariance between wind and waves, and must be considered on a location-by-location basis [16]. Regional case studies in reducing variability have been carried out for locations in California, Denmark, Ireland and Australia [17–20], but prior to this article had not been considered for the Canary Islands: a combined study of wind and wave resource in Tenerife [10] did not include temporal variation, smoothing or joint statistics.

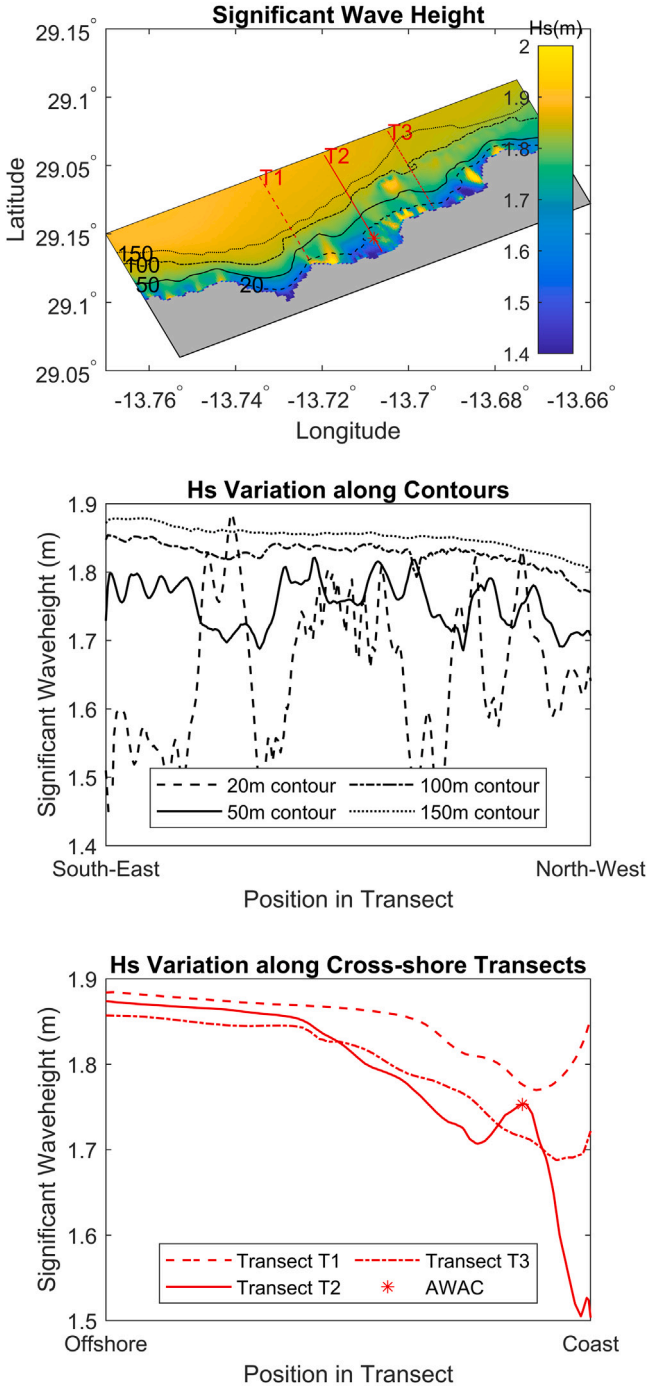

Fig. 7. Variation of significant waveheight along depth contours (middle plot) and cross-shore transects (lower plot). The upper plot shows the spatial distribution over the inner model domain, as well as the locations of the transects and contours. The black asterisk shows the AWAC location which is the area of most interest for energy extraction.

1.3. Structure of the article

This article presents a detailed exploration of the nearshore wave resource in the most energetic part of the Lanzarote coastline, by means of a high-resolution nested SWAN model (described in Section 2), validated by sensor data (Section 3). To meet the particular challenges of modelling this volcanic archipelago, for which deep water persists until less than two kilometres from the coastline, a 50 m structured grid is nested into a larger 1.5 km resolution grid, which is in turn

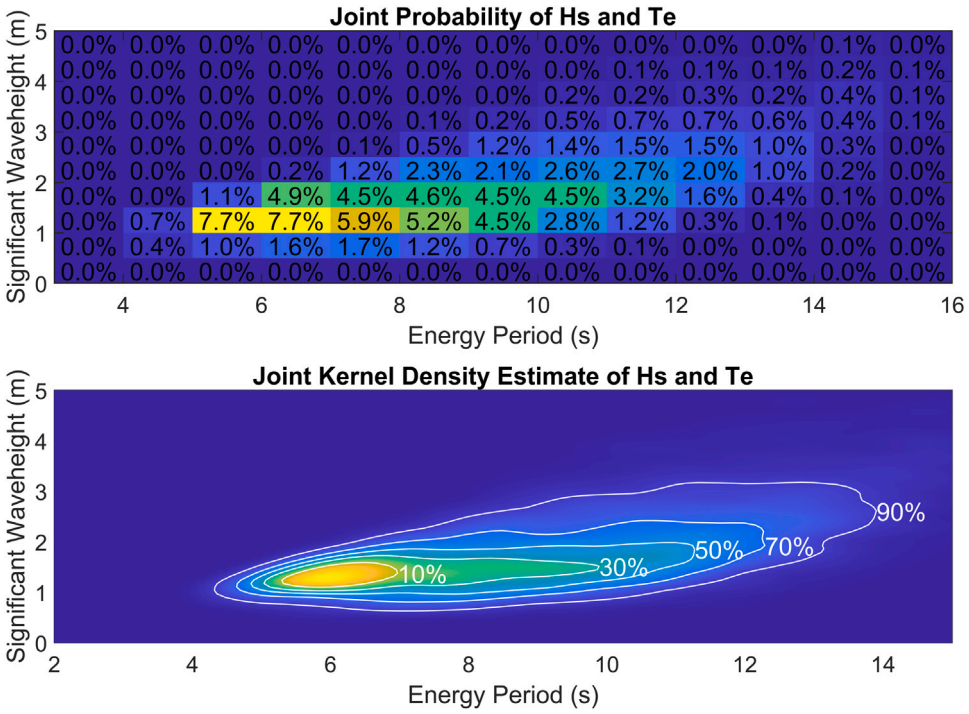

Fig. 8. Joint probability of significant waveheight and energy period at a potential energy extraction location. The upper image shows a table with percentages for each binned seastate combination, while the lower image shows a joint kernel density estimate with percentage exceedence contours.

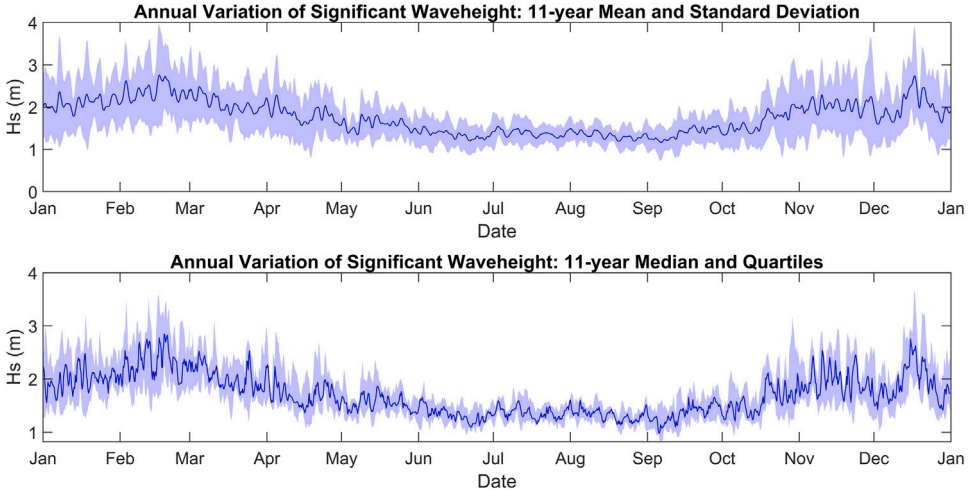

Fig. 9. The solid line in the upper plot shows the eleven-year mean value for each timestep, to give an "average" year: the shaded area shows one standard deviation above (and below) this mean. In the lower plot, the solid line is the median value, and the shaded area is between the lower and upper quartiles.

driven by directional spectra varying spatially along the boundary, obtained from a global model. Unlike previous treatments (such as [4,7] discussed above), this allows full characterisation (in Section 4) of the considerable spatial variation of the nearshore resource arising from bathymetric features. The Lanzarote site is dominated by long-distance swell waves, and Section 4 goes on to investigate the extent of decoupling from local wind, and the dependence of the overall coefficient of variability on the relative proportions of wind and wave energy, to determine an optimum energy mix for this location. Analyses of wind-wave covariance depend fundamentally on location [16] and have not previously been carried out for the Canary Islands.

Finally, Section 5 uses the model data to explore a novel non-physics-based method for determining wave parameters at a given location, allowing the hindcast to be extended backwards in time by several decades at negligible computational cost, and allowing the possibility of forecasting. Unlike surrogate modelling techniques requiring a systematic exploration of input parameter space such as [21,22], we demonstrate that one can achieve an accurate reconstruction from pure timeseries data using simple multilinear regression.

2. Methods

The wave hindcast consists of a nested pair of SWAN models [6,23], the outer of which is nested within the global ECMWF ERA-5 WAM wave model [24]. Both SWAN and WAM are third generation spectral wave models: such spectral wave models are used as standard in wave

energy resource assessment and underpin the analyses in [4,5,7–10] discussed above. The underlying physics in such models is discussed in Section 2.1, and is described in detail in [6,23]. Further information on the use of spectral wave modelling in wave energy resource assessments may be found in [25].

2.1. Spectral wave models and their outputs

Third generation spectral wave models such as SWAN simulate the evolution of wave spectra using the Wave Action Conservation Equation [26]:

$$\sigma\left\{\frac{\partial}{\partial t}\left(N(\mathbf{x},\sigma,\theta,t)\right)+\nabla.\left[\mathbf{v}N(\mathbf{x},\sigma,\theta,t)\right]\right\}=\begin{array}{cc} s_{\text{wind}} & \text{Wind Forcing}\\ +s_{\text{wcap}} & \text{Whitecapping}\\ +s_{\text{bot}} & \text{Bottom Friction}\\ +s_{\text{surf}} & \text{Wavebreaking}\\ +s_{\text{nl}} & \text{Nonlinear Interactions}\end{array} \tag{1}$$

Here, the depth-averaged action density $N(\sigma,\theta,\mathbf{x},t)=\frac{E(\sigma,\theta,\mathbf{x},t)}{\sigma}$, where $E(\sigma,\theta,\mathbf{x},t)$ is depth-integrated energy density (i.e. the directional spectrum), σ is angular frequency (in a reference frame moving with current), θ is direction, $\mathbf{x}$ is horizontal position, and t is time.[1] The propagation velocity $\mathbf{v}$ and differential operator ∇ act in four-dimensional phase space: two spectral dimensions (σ and θ) and two spatial dimensions ($\mathbf{x}$). The $\nabla.(\mathbf{v}N)$ term includes shoaling, depth- and current-induced refraction, and can be modified to incorporate diffraction. WAM [27] was originally developed to model the generation and deepwater propagation of ocean waves. SWAN ("Simulating WAves Nearshore") was historically designed for smaller-scale simulations of nearshore wave transformations, but is also suitable for large-scale deepwater models [28].

The energy density $E(\mathbf{x},\sigma,\theta,t)$ may be output at a given position and time within the model. At a given location in the model, SWAN can also output the *energy transport vector*, whose Cartesian components are given by

$$P_{x,y}=\rho g\int c_{x,y}(\sigma)E(\sigma,\theta)\mathrm{d}\sigma\mathrm{d}\theta \tag{2}$$

where $c_{x,y}$ is the x- or y- component of the group velocity, and we are henceforth suppressing the explicit $\mathbf{x}$ and t dependence from the notation. The magnitude of (2) gives the rate of energy transport (and hence the theoretical power available to a wave energy converter) per unit wavefront, thereby allowing a device-agnostic measure of wave resource.

Integrating the spectral density $E(\sigma,\theta)$ over the wave direction θ gives the *omnidirectional spectrum*, which is conventionally written $S(f)$, in terms of frequency f in Hertz. The spectral moments

$$m_n=\int S(f)f^n\mathrm{d}f \tag{3}$$

of $S(f)$ are used to calculate significant waveheight H_s and energy period T_e:

$$H_s=4\sqrt{m_0},\qquad T_e=\frac{m_{-1}}{m_0}. \tag{4}$$

These parameters provide a characterisation of the seastate, both operational and extreme, and may be used in conjunction with a device power matrix to estimate yield from a wave energy converter. In deep water, H_s and T_e may also be used directly to give a measure of theoretical power available. Since $c_g\simeq\frac{gT}{2\pi}$, definitions (3)–(4) allow the magnitude of (2) to be rewritten in the simplified deepwater form:

$$P_0\simeq\frac{\rho g^2}{64\pi}H_s^2T_e. \tag{5}$$

[1] Although we are operating in the frequency domain, the spectral quantities can vary over timescales of order minutes or hours.

However, this case study concerns *nearshore* energy extraction in shallow or intermediate water depths, so the SWAN-calculated power values presented in Section 4.2 are obtained from the full spectral formula (2).

2.2. The Lanzarote model

The Lanzarote model consists of the nested pair of outer and inner model domains shown in Fig. 2. The choice of model domain reflects the bathymetry. As a volcanic island, Lanzarote has no continental shelf, with deep water (>1000 m) found very close to the coast, followed by extremely rapid bathymetric change. To capture this variation requires high spatial resolution, and consequently a limited spatial extent, focussed on the area of interest for wave energy exploitation: the north-west coast of Lanzarote around La Santa. This is nested into a coarser outer model, which was in turn driven by 2D spectral output from the global ERA-5 WAM wave model.

The outer model is a structured grid of 1.5 km cell size, incorporating the islands of Gran Canaria, Fuerteventura and Lanzarote, of dimensions approximately 300 × 150 km. Bathymetry data from EMODNet [29] was used, in conjunction with local multibeam survey data for the deployment site for the inner model. In each case, the bathymetry resolution exceeded the model resolution: the EMODNet bathymetry resolution was $\frac{1}{16}\times\frac{1}{16}$ arcminutes, while the local multibeam survey yielded elevation maps at <1 m resolution.

The boundary is chosen to correspond exactly with twelve grid-points of the global ERA-5 model, which produces hourly directional spectral output interpolated onto a regular 0.5° × 0.5° grid from its native Gaussian discretisation. These are discretised into 24 equally-spaced directional bins, and 30 frequency bins, starting at 0.03453 Hz and increasing geometrically with $f(n)=1.1\times f(n-1)$ up to 0.5478 Hz. Forcing the model with ERA-5 directional spectra at multiple points may be achieved by converting the downloaded spectral data to the same format as SWAN nested output, then using the BOUNDNEST command. For the outer model, the spectral coverage and resolution is increased to 48 directional bins and 35 geometrically spaced frequency bins from 0.02358 Hz to 0.54775 Hz ($T\sim1.8$–42.4 s). It is run in non-stationary mode with a 12 min timestep, using a first-order upwind propagation scheme.

The inner model is oriented along the Lanzarote coast (at an angle of 25.35° with respect to lines of latitude), extending 11.7 km long-shore and 4.4 km cross-shore (Fig. 2b). The inner model increases spatial resolution to 50 m and directional resolution to 3° (120 directional bins), but uses the same 35 frequency bins as the outer model. The boundary and wind conditions may be considered to be constant over the propagation time from offshore boundary to coastline (a short distance of order 3 km), so the inner model is implemented as a series of stationary simulations corresponding to the output timesteps, as recommended by SWAN for small, high-resolution models with relatively large timesteps. The nested output from the outer model offers spectra at 8 long-shore intervals.

Wind forcing is from the ERA-5 model, providing hourly data at a 0.25° resolution. Time varying water level was not included in the outer model, where water depths in the region of interest were never less than 200 m, but was initially included in the inner model using TPXO9v2a data [30] using the TMD Matlab toolbox [31]. Following a sensitivity analysis, tidal current was found to have negligible effect on simulated wave properties across the computational domain, while adversely affecting model run times, and was consequently omitted.

3. Validation and sensitivity

A Nortek Signature 1000 ADCP was deployed for three months, between the 30th December 2019 and the 29th March 2020, at 29°5′56″N, 13°41′17″W, a location with, on average, 13.5 m water depth. Wave

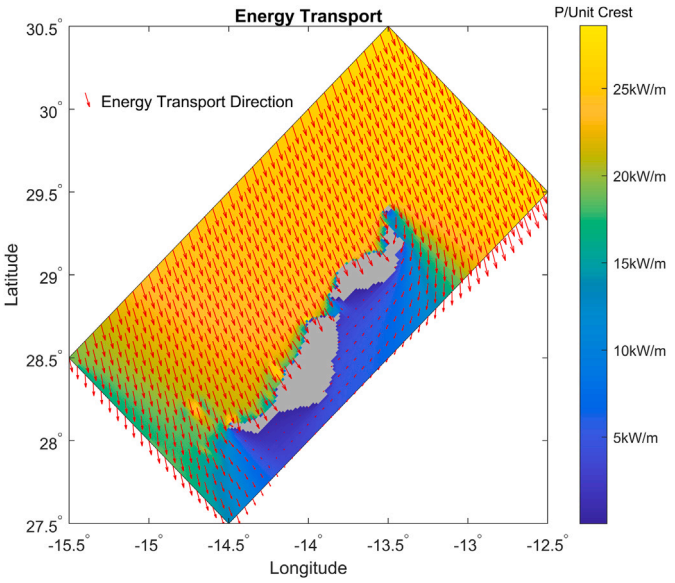

Fig. 10. Eleven-year (2010–21) mean rate of energy transport from the outer SWAN model, calculated using (2). The shading shows the magnitude of the energy transport, and the red arrows show the direction. In the northern part of the domain, there is little spatial variation – almost up to the coastline – with fluxes of approximately 25 kW/m.

parameters were reported every hour: of the frequency-domain parameters available, the significant wave height H_s and peak period T_p were used for model validation.[2]

Hourly output from the inner SWAN model for the same time period, providing SWAN hindcast H_s and T_p for each of the 2100 pairs of AWAC-measured values. Timeseries for AWAC-measured and SWAN-simulated H_s and T_p, and scatter plots showing the correspondence between measured and modelled values are shown in Fig. 3. The joint occurrence frequency of each $H_s - T_p$ pair is shown in Fig. 4.

For the significant wave height, the SWAN model had a bias (difference between the mean values) of −0.03 m, a scatter index (root mean squared error normalised by the mean) of 14.4%, and a Pearson correlation coefficient (r) of 0.91 ($r^2 = 0.83$). For the peak period, the bias was 0.1 s, scatter index 9.7% and $r = 0.73$ ($r^2 = 0.53$).

For the validation, the (stationary) inner model had been set up to create hourly output, matching the availability of the AWAC data. However, the models are driven by ERA-5 *global* wind and boundary wave data: although this is available with an hourly timestep, the metocean conditions obtained from this model do not vary sufficiently rapidly to justify an hourly timestep for the full hindcast. To illustrate this, hourly values for significant waveheight were generated in two ways for a sample time period: direct evaluation by running an hourly SWAN model, and interpolation from a six-hourly model. The results in Fig. 5 show negligible difference between the direct and interpolated hourly data. The RMS error in the hourly timeseries interpolated from the six-hourly SWAN runs, compared to the timeseries obtained by running an hourly SWAN model, is 0.00052 m, or 0.02% of the mean significant wave height. Therefore, running the inner model every six hours has minimal impact on the fidelity of the output, while allowing computation time to be reduced by a factor of six.

[2] The energy period T_e was not provided in the AWAC data, but quality indices derived from T_p are assumed to indicate comparable model performance in calculating T_e.

4. Results

4.1. Seastate characterisation

The outer and inner models were run for an eleven year period from the 1st January 2011 to the 31st December 2021. Eleven-year mean values for significant waveheight and energy period are shown in Fig. 6, with red arrows indicating the mean wave direction at selected points. Due to the lack of a continental shelf, the wave properties remain almost constant from the north-western model boundary to the north-west coast of Lanzarote, with the prevailing wave direction coming from the North, and reduced wave action on the south-eastern coast. Despite this lack of variation, the outer model still plays an important role in transforming the globally modelled spectral wave conditions from the north-western boundary. It allows us to drive the model from only ERA-5 data points located in regions of limited spatial variability, away from any landmasses or sub-grid-scale variations (the south-eastern boundary is closer to land, but this does not affect the wave conditions at the region of interest around La Santa). The spatial dependence of the 11-year averaged significant waveheight and energy period for the *inner* model exhibits very gradual variation, which becomes rapid around 1 km from the coastline. The behaviour of significant waveheight is plotted along depth contours and cross-shore transects in Fig. 7.

While Figs. 6–7 showed the spatial variation of time-averaged significant waveheight and energy period, the remainder of this section considers the time dependence of these quantities at the location of most interest for wave energy extraction: the AWAC validation location, shown as a black asterisk in the inner model on Fig. 6, close to La Santa.

To characterise the temporal variability at this location, eleven-year hourly joint occurrence tables, and bivariate kernel density estimates, are shown in Fig. 8. The joint probability table can be combined with a device power matrix to estimate annual energy yield. The KDE plot shows correlation between significant waveheight and energy period: in this swell-dominated location, the largest waves occur in seastates with the largest periods.

Fig. 9 shows averaged intra-annual variation of significant waveheight, constructed by comparing corresponding dates and times across the eleven year hindcast. First, a 24-hour moving mean is constructed from the six-hourly significant waveheight values, for the whole eleven year hindcast period. This is then converted into a single "averaged" year, by calculating the mean, median, standard deviation, first and third quartiles for each timestep across the eleven years of hindcast data. So, for example, the "Jan 1st, 06:00" step is an average of the seastates at every Jan 1st 06:00 for each of the years 2011–2021.

Maxima occur in February and December, but the seasonal variability is less pronounced than one would find in higher latitude regions (e.g. [32]). The timeseries of parameters such as significant waveheight, energy transport, and a selection of peak and mean periods is available in the supplementary files to this paper: a full definition of the output quantities is available in [33].

4.2. Power

For a given device, the annual energy yield may be predicted by combining probability distributions such as those presented in Fig. 8 with the power matrix of the device in question.

Alternatively, for site characterisation, a device-agnostic measure of theoretical yield may be obtained from the magnitude of the energy flux calculated from the directional spectrum using Eq. (2) (or the deepwater approximation calculated from the spectral parameters using Eq. (5).) The SWAN model can directly output the components of the energy transport (2), which is valid for all water depths. The values in the northern part of the outer domain are relatively uniform, almost up to the edge of the landmasses.

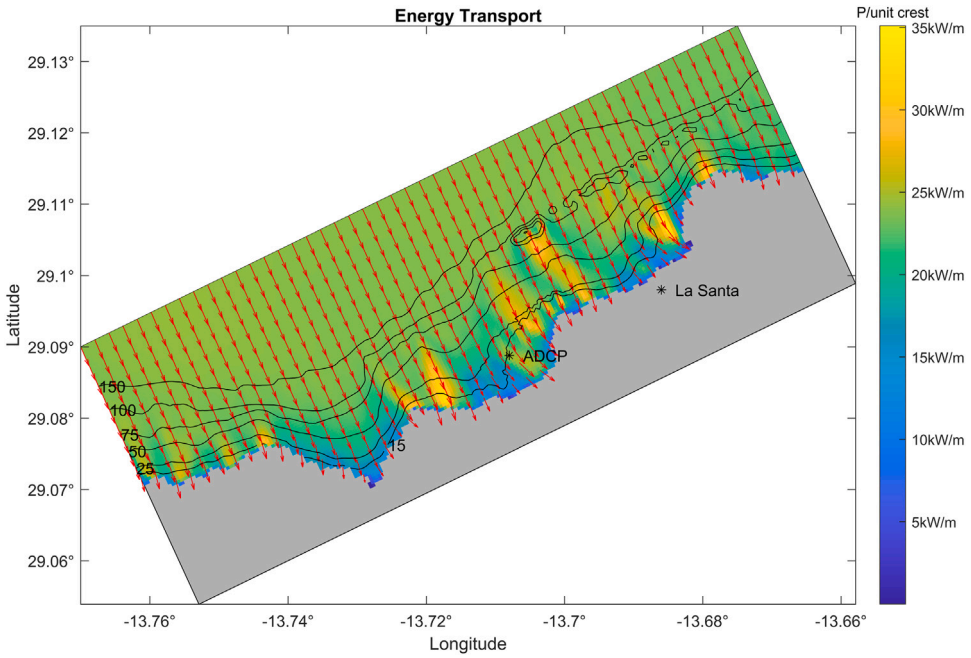

Fig. 11. Eleven-year (2010–21) mean rate of energy transport from the inner SWAN model, calculated using (2). The shading shows the magnitude of the energy transport, and the red arrows show the direction. Bathymetric contour lines are shown in black. Local areas of significantly elevated energy transport can be seen.

Fig. 10 shows eleven-year averaged deep-water wave energy transport for the outer model; the corresponding values for the inner model are in Fig. 11. The shading indicates the magnitude of the energy flux, while arrows overlaid on a coarser grid indicate direction. Taking both plots together, the power propagating from the North is virtually uniform (with fluxes of around 25 kW/m) until the 100 m contour line (approximately 2 km from the coast), and then begins to exhibit more local-scale variability, with the bathymetric variation causing some focussing into local high-energy "hotspots".

The energy transport of approximately $\simeq$ 25 kW/m in the north coast of Lanzarote is somewhat lower than the combined hindcasts and forecasts for the HIPOCAS model reported in [4], where annual averaged power between 1958 and 2008 reached 30kW/m. However, this was obtained from the deep water expression (5) by taking the approximation $T_e \simeq T_p$. For the grid points in Fig. 10 the true relationship is found to be closer to $T_e \simeq 0.8T_p$.

4.3. Potential for co-location

By sharing infrastructure (e.g. cabling), levelised cost can be reduced by *co-locating* two or more offshore renewable energy technologies [34]. Two candidate technologies for co-location, especially due to the high cost of wave energy, are offshore wind and wave energy [18]. To diversify generation times, suitable regions require the wind and wave resource to be either uncorrelated, or for there to be a phase lag between the timeseries. This is more likely to occur in regions that are dominated by swell waves, as opposed to local wind seas.

Fig. 12 shows the phase relationship between wind and wave power at the model point corresponding to the AWAC location: 29°5′56″N, 13°41′17″W. For a given time lag, the wave power timeseries was shifted relative to the wind by the appropriate time period, and then the Pearson correlation coefficient was calculated. The maximum correlation occurs for a five-hour shift. This is due to the very large Atlantic fetch at the location, in contrast to the one-hour phase shift observed in the North Sea [18].

The existence of such a phase shift is beneficial for grid resilience and power quality. Furthermore, a low absolute value of the correlation coefficient is an indicator of the profitability of resource smoothing [16]: here the correlation coefficients are very low, never exceeding 0.25. This relative lack of correlation may be seen in Fig. 13, which shows that time periods with large wave power do not regularly correspond with those of large wind power. The shape of the contours is very different to, for example, those in Fig. 8 which shows the relationship between two relatively well-correlated quantities. Swells arriving at Lanzarote may have originated many hundreds of miles away, and the wind field associated with their generation may not arrive in the same form, and will not arrive at the same time as the waves.

The low correlation between wind and wave power means that grid and storage requirements may be reduced by considering hybrid developments in Lanzarote, by reducing overall variability of power output. This can be seen in Fig. 14, which plots temporal variation of wave and wind power over different time periods in 2021 (the whole year, the first six months and the month of February), and shows that periods of higher (and lower) wind and wave power do not regularly coincide.

Consider a hybrid wind-wave development with $W\%$ of the overall lifetime power supplied by wind. The time dependence of the combined power is given by

$$P_{\text{combined}}(t) = \frac{W}{100}\frac{P_{\text{wind}}(t)}{\overline{P}_{\text{wind}}} + \frac{100-W}{100}\frac{P_{\text{wave}}(t)}{\overline{P}_{\text{wave}}}, \tag{6}$$

where a bar indicates mean. The coefficient of variation (COV), defined as the standard deviation divided by the mean, is commonly used to quantify variability in energy resource (see, for example, [4,35,36]). Fig. 15 shows how the wind-wave mix affects variability, using the COV calculated from six-hourly values of the combined wind and wave power given by (6) for 2011–2021. The COV for 100% wave power is 1.1, and the COV for 100% wind power is 1.0. However, a 55% wind, 45% wave combination reduces this to 0.8, potentially leading to improved power quality, less requirement for storage, and less pressure on the grid.

5. Extending to multi-decadal time scales

The eleven-year hindcast used a physics-based deterministic (SWAN) model of the Lanzarote area to transform time-varying input data (such

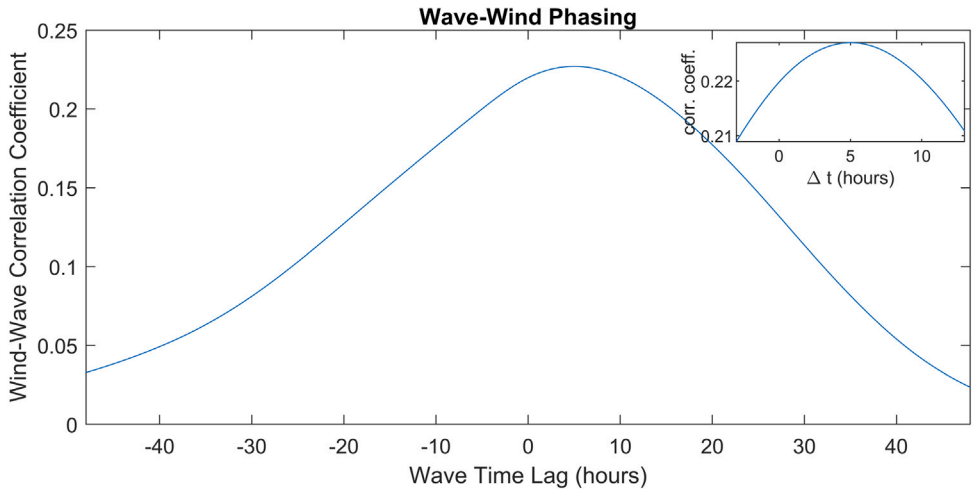

Fig. 12. Dependence of time shift between wind and wave on correlation between the power data timeseries from 2011–2021. The location of the maximum implies that on average the wave behaviour lags five hours behind the wind.

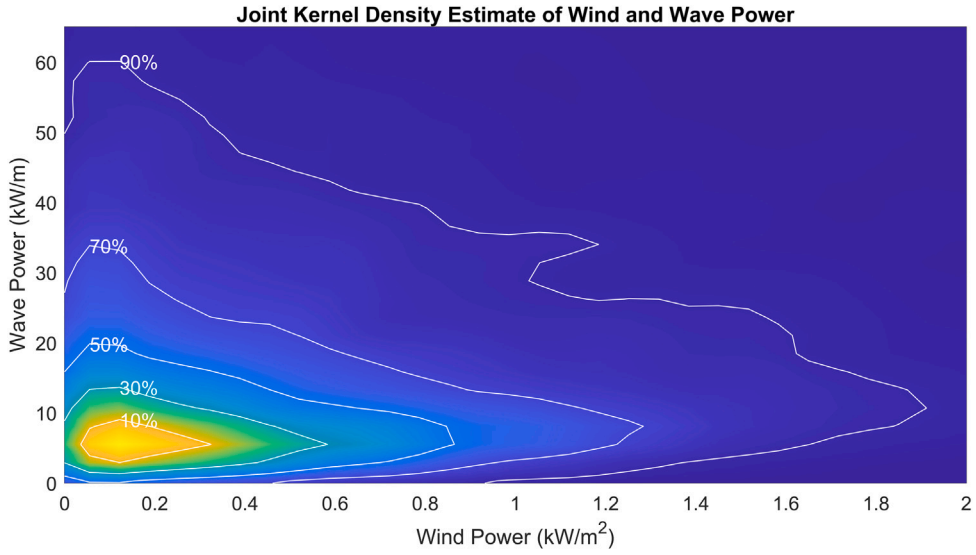

Fig. 13. Joint kernel density estimate of wind and wave power. More energetic seastates are not highly correlated with larger values of wind power.

as offshore wave spectra, local wind fields and water level) to output wave conditions at the nearshore area of interest.

We now seek to determine if the hindcast data can allow us to construct a simple empirical correlation-based model expressing particular output parameters in terms of a smaller subset of input data, thereby allowing the hindcast to be extended in time without additional SWAN modelling.

Our hypothesis is that an output parameter Q (such as significant waveheight) at a given nearshore location $\mathbf{x}_q$ may be approximately written as an empirical function of M quantities (either recognised parameters such as energy period, or components of a spectrum) evaluated at N combinations of offshore location and time, i.e.

$$Q(\mathbf{x}_q, t) \simeq F\Big(P_1(\mathbf{x}_1, t-\tau_1), \ldots, P_M(\mathbf{x}_N, t-\tau_N)\Big) \tag{7}$$

where F is some unknown function to be determined empirically, t is time, and τ_n is a time delay to allow for conditions to propagate from $\mathbf{x}_n$ to $\mathbf{x}_P$. If the input parameters $P_m(\mathbf{x_n}, t-\tau_n)$ can be obtained from global datasets, then one would be able to extend a local hindcast over multiple decades without explicit calculation, with negligible computational effort. It would also allow straightforward seastate *forecasting* using operational global forecast models.

Specialised machine-learning or Bayesian approaches may facilitate the generation of sophisticated "surrogate models" for this purpose from a small, strategically selected training dataset [21,22]. By contrast, we seek to determine a lower bound for the fidelity of such models, by developing the simplest possible approach based on straightforward interpolation of a small number of input parameters.

For this simple example, we shall correlate ECMWF global data at a single "Driving" datapoint (an offshore location at 30°N, 14°W), with SWAN output data at the nearshore "Evaluation" point 105 km away (and evaluated one hour later) at 29°5′56″N, 13°41′17″W, in 13.5 m water depth, coinciding with the ADCP deployment location, as shown in Fig. 16.

The ERA-5 data used for this example was significant wave height, mean wave period, and significant height of total swell. In terms of Eq. (7), $\mathbf{x}^q$ is the ADCP location (the Evaluation Point), and $N = 1$ with $\mathbf{x}^1$ as the Driving ERA-5 datapoint at 30°N, 14°W, and τ_1 as 1 h. We use three parameters for driving data, so $M = 3$ with P_1, P_2 and P_3 being the ERA-5 significant wave height, mean wave period, and significant height of total swell. Two separate models were created: one for which the output parameter Q was the significant waveheight, and a second model for which Q was the energy period.

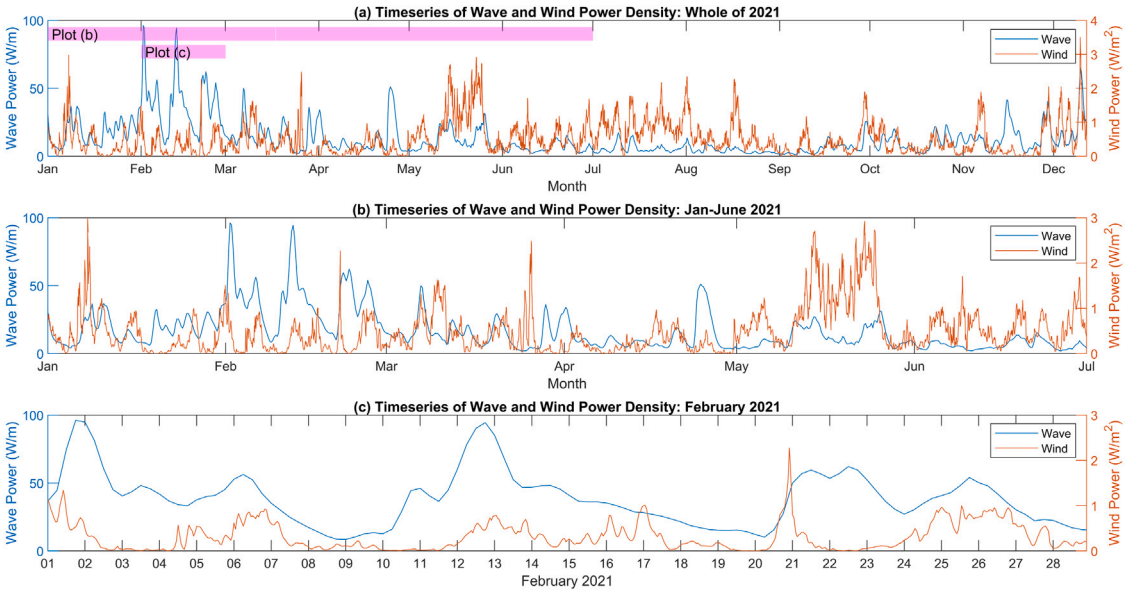

Fig. 14. Timeseries of wind and wave power, over different time periods in 2021. Episodes of large wave and wind power do not regularly coincide. The sustained period of high wave power in February did not correspond to increased wind energy, whereas the stronger winds experienced in late May did not show heightened wave action.

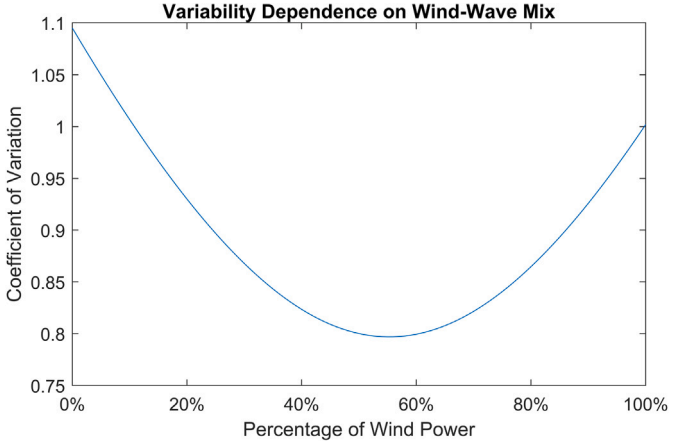

Fig. 15. Dependence of coefficient of variability ("COV", defined as standard deviation divided by mean) on the proportions of wind and wave. While the COV for 100% wave power is 1.1, and the COV for 100% wind power is 1.0, a 55% wind, 45% wave combination reduces this to 0.8.

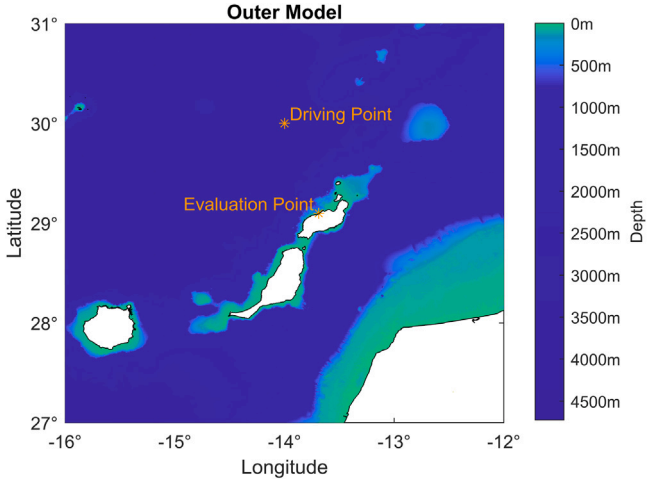

Fig. 16. The "Driving" and "Evaluation" points for our correlation-based model. ECMWF wind and wave parameters at the offshore Driving Point are correlated with significant waveheight and energy period at the nearshore Evaluation Point based on ten years of the SWAN hindcast. These correlations are then used to predict the behaviour at the Evaluation Point for a further year, using only that year's ECMWF data at the Driving Point, without recourse to any further SWAN modelling.

In each case F was encoded as a Matlab `scatteredInterpolant`. The fitting data at the Evaluation Point $\mathbf{x}^q$ came from ten years of six-hourly timesteps from the SWAN hindcast (January 2011 – December 2020), i.e. evaluated at 00:00, 06:00, 12:00 and 18:00 daily. The corresponding ERA-5 parameters were evaluated at 23:00, 05:00, 11:00 and 17:00 each day at the global model data point at 30°N, 14°W, to account for the hour's delay time τ. Each timestep was treated as an independent point in the scattered interpolant. By using data derived from timeseries, one will automatically have more densely populated regions in parameter space, corresponding to the most common combinations of seastate and atmospheric parameters. This means that the model should be more accurate in the most commonly encountered conditions, but may require additional fitting data to successfully model extremes.

The eleventh year of the hindcast, 2021, was used for validation. Taking the ERA-5 timeseries for the significant wave height, mean wave period, and significant height of total swell at the offshore point, the scattered interpolant created from the ten year hindcast was used to estimate a new timeseries for the nearshore significant waveheight without recourse to the 2021 SWAN model. This was then compared with the actual SWAN output, for validation. The process was then repeated for the energy period.

Fig. 17 shows the timeseries of significant waveheight and energy period for the 2021 validation period, comparing the values directly calculated in SWAN with those obtained by using the 2011–2020 hindcast data to correlate the offshore parameters with the nearshore values. Fig. 18 compares the single and joint statistical distributions of hindcast parameters with the directly calculated and reconstructed values. The reconstructed significant waveheight had a scatter index of 6.92%, a bias of 0.002 m and a correlation coefficient of 0.981. The reconstructed energy period had a scatter index of 5.92%, a bias of −0.015 s and a correlation coefficient of 0.978.

This simple demonstration of principle generated a satisfactory reconstruction for H_s and T_e based only on three offshore parameters and a Matlab scattered interpolation method. One possible refinement of the

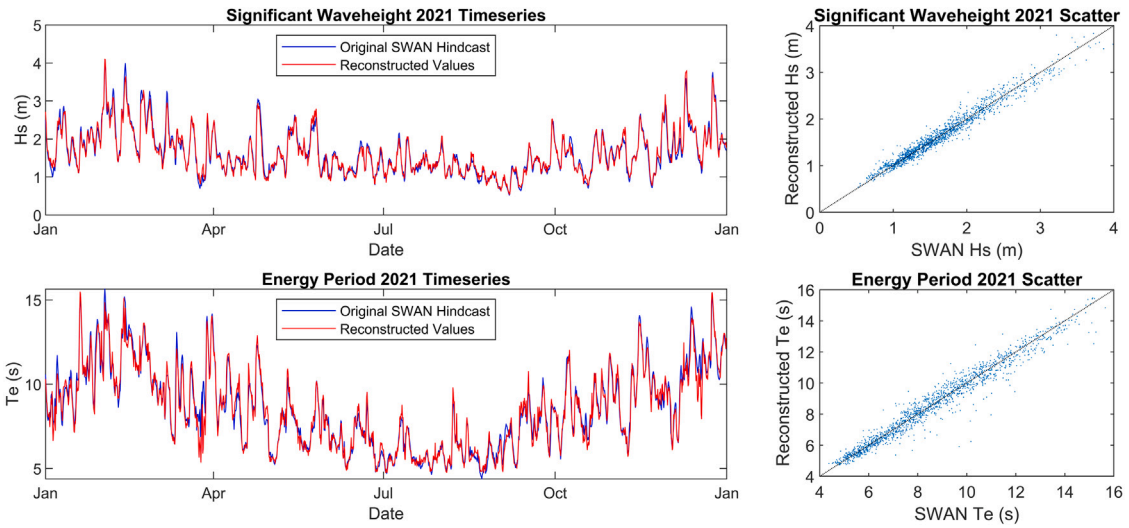

Fig. 17. Timeseries and scatter plot comparing the significant wave height and energy period calculated directly using SWAN with the reconstruction generated by correlating ERA offshore data with the SWAN outputs from the previous ten years. Scatter indices for H_s and T_e were 6.92% and 5.92% and bias was negligible.

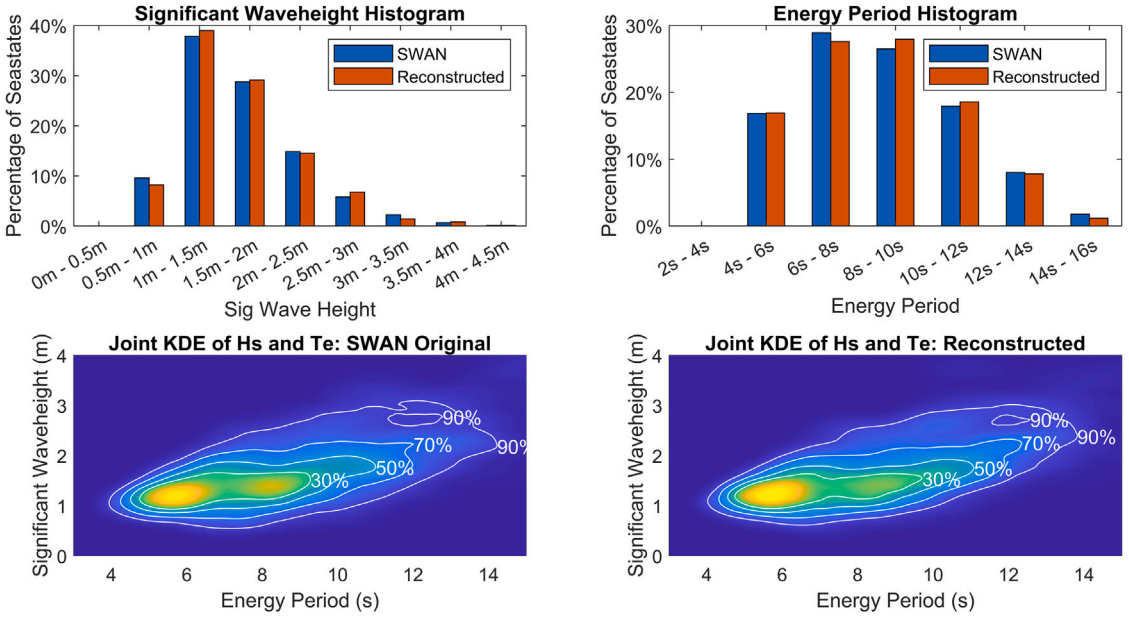

Fig. 18. Significant waveheight and energy period histograms, and joint probability density for the directly modelled and reconstructed 2021 data. The similarity implies that a simple reconstruction technique may be used to extend the hindcast time period to that of the underlying global dataset.

method might involve partitioning into wind-sea and swell, fitting each separately (also incorporating direction) and then recombining at the end. A more sophisticated fitting method using more seastate variables combined with elements of machine learning may also offer further increases in accuracy.

To test how much of the SWAN hindcast is needed for a satisfactory multivariate interpolation, the reconstruction was repeated for different quantities of fitting data. In each case, the nearshore conditions for 2021 were repeatedly reconstructed, using interpolants generated from different lengths of SWAN hindcast, ranging from 2011 alone, to the full ten years from 2011 to 2020. The dependence of the quality indices on fitting record length shown in Fig. 19. For this simple reconstruction, a time period of three to four years is adequate for low scatter indices and high correlation coefficients, with extra data only leading to a very gradual improvement. However, refining the method by utilising additional ERA-5 parameters would require the full dataset, to ensure a more complete coverage of parameter space (or else a more strategic approach to generating the SWAN models representing a range of seastate conditions).

Returning to the ten-year dataset, the same validated Matlab interpolant was used to extend the hindcast backwards in time to 1959, to match the availability of the global ERA-5 data. The 63-year equivalents to the eleven-year output from Figs. 8 and 9 are shown in Figs. 20 and 21.

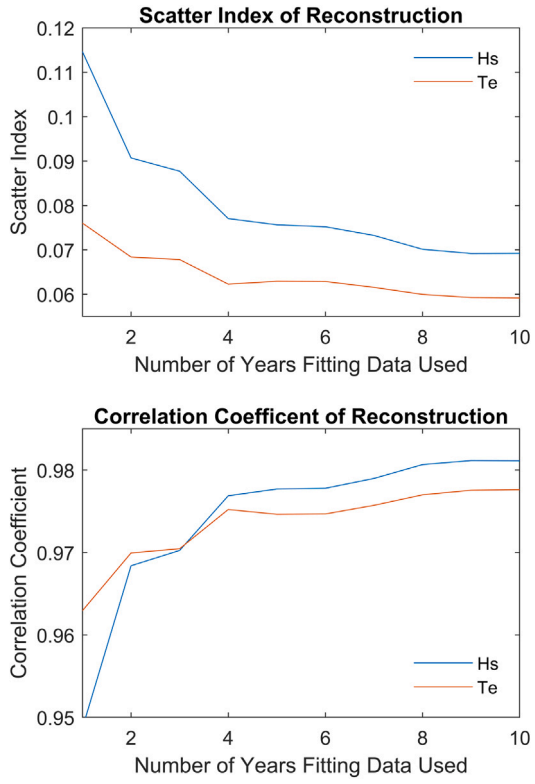

Fig. 19. Fidelity of the simple scattered interpolant reconstruction technique as a function of the length of the SWAN hindcast used as data.

6. Discussion and conclusion

Geographically and socially, Lanzarote is ideally placed for increased exploitation of wave energy. Authorities have demonstrated a commitment to reducing fossil fuel dependence by funding grid improvements and facilitating demonstrator deployments such as the Bombora site in La Santa, to take advantage of the energetic wave resource resulting from uninterrupted exposure to the Atlantic fetch.

An analysis of global model output at deepwater grid points off the north of the island shows a large energy density [4]. However, a detailed description of the local wave climate requires global models to be coupled to nearshore simulations. In this article, SWAN models were nested into the global ECMWF ERA-5 wave model. The boundary of the outer SWAN model was driven by full directional wave spectra, at the same 0.5° resolution as the ERA-5 global data. This fed a high-resolution (50 m grid) local model in the vicinity of the Bombora development at La Santa. This approach best exploits the accuracy and fidelity of the validated global model, by transforming ERA5's detailed, spatially varying, fully spectral boundary conditions towards the inner boundary, without having to re-model large sections of sea. Validation at the proposed wave extraction site showed good agreement with data from a three-month AWAC deployment. Lanzarote has no continental shelf, with deep water giving way to very rapidly varying bathymetry close to the coast. The modelling shows that the significant waveheight and energy period also exhibit very little spatial variation until a few kilometres away from the coastline, followed by rapid local variations. The power density, calculated from H_s and T_e, will therefore also remain constant in the same region, followed by a rapid reduction a short distance from the coast. This extreme local variability cannot be captured by a 0.5° scale global model. High-resolution nearshore modelling is essential for resource characterisation where changes in wave properties may be too rapid to be accommodated within a coarser grid. In swell dominated seas, care must also be taken to correctly characterise power in terms of the energy period.

The wave resource varies seasonally, with higher powers between November and April, though the variation is less than one would find at higher latitudes. The domination of swell is favourable for energy extraction, with a correlation between larger significant waveheights and longer energy periods, resulting in larger power densities. The domination of swell also means that there is low correlation (and a five-hour phase lag on average) between wave power and local wind. This is beneficial for combined wind-wave developments, resulting in less variability than wave or wind alone. The reduction in resource in summer may be further balanced by adding solar power to the energy mix.

Timeseries of significant waveheight, energy period, and hence power, may also be extended by a relatively straightfoward correlation and interpolation method, using the eleven-year hindcast (or a shorter subset thereof), in conjunction with three parameters from the global model at a neighbouring offshore location. Triplets of the offshore parameters are correlated to modelled significant waveheight, and separately to modelled energy period for several years' worth of SWAN model run. This can be used to extend the timeseries, since the ERA-5 dataset provides global parameters extending back to 1959. It may also be combined with the operational forecast to provide forecast estimates of the seastates. More datapoints are available for most common seastates, meaning this fitting methods works well for characterising operational conditions, but may be less successful at estimating extreme behaviour.

CRediT authorship contribution statement

David Christie: Conceptualization, Methodology, Formal analysis, Writing – original draft, review & editing, Visualization. **Simon P. Neill:** Conceptualization, Writing – review & editing, Funding acquisition. **Peter Arnold:** Investigation, Writing – review & editing.

Declaration of competing interest

The authors declare that they have no financial interests/personal relationships which may be considered as potential competing interests: David Christie, Simon Neill, Peter Arnold.

Acknowledgements

We are grateful to the two anonymous reviewers who provided useful feedback on an earlier version of the manuscript. David Christie and Simon Neill acknowledge the support of SEEC (Smart Efficient Energy Centre) at Bangor University, part-funded by the European Regional Development Fund (ERDF), administered by the Welsh Government. Peter Arnold acknowledges the assistance of Ecos Estudios Ambientales *y* Oceanografia of Gran Canaria in the provision of the bathymetric and ADCP data used in this project on behalf of Bombora Wave Power Europe Limited.

Appendix A. Supplementary data

Supplementary material related to this article can be found online at https://doi.org/10.1016/j.renene.2023.02.126.

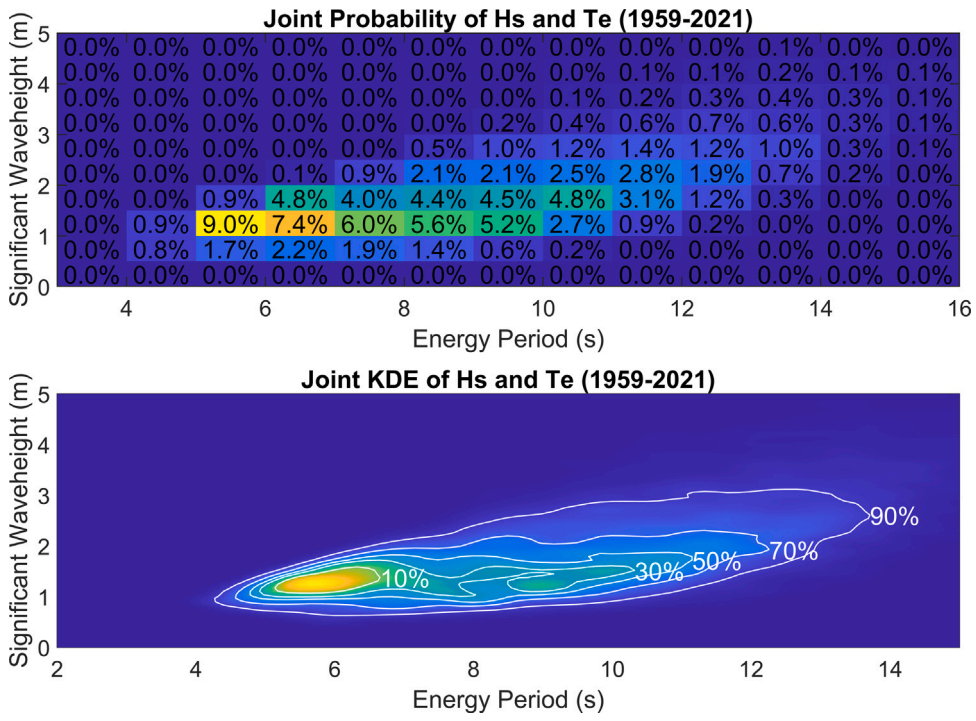

Fig. 20. Joint probability of nearshore significant waveheight and energy period for an extended 63-year hindcast created by correlating offshore seastates with the SWAN model output. The corresponding directly calculated 11-year SWAN model result was given in Fig. 8.

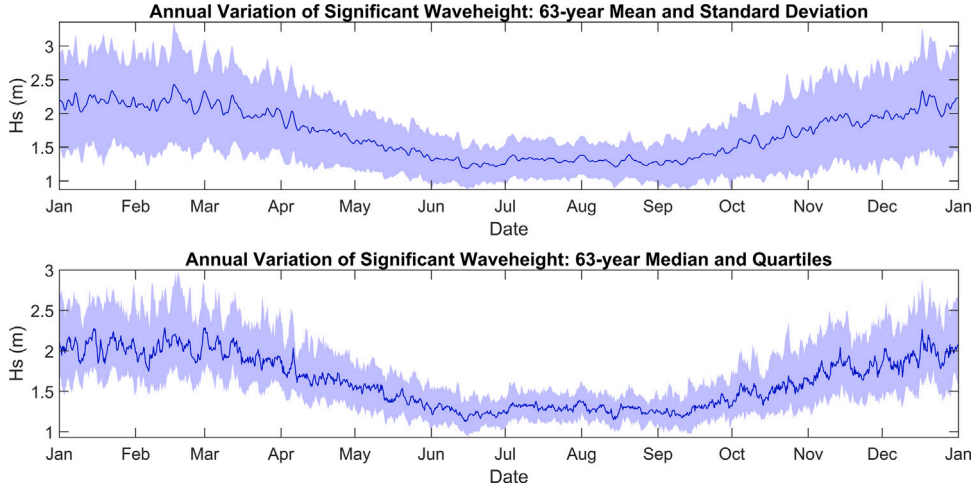

Fig. 21. The 63-year mean and median significant waveheights for each date, with the shaded areas showing standard deviation (top plot) and the region between the 25th and 75th percentiles (bottom plot). This is the 63-year extended version of Fig. 9.

References

[1] Assessing the global wave energy potential, in: 29th International Conference on Ocean, Offshore and Arctic Engineering: Volume 3 of International Conference on Offshore Mechanics and Arctic Engineering, http://dx.doi.org/10.1115/OMAE2010-20473.

[2] O. Edenhofer, R. Pichs-Madruga, Y. Sokona, K. Seyboth, S. Kadner, T. Zwickel, P. Eickemeier, G. Hansen, S. Schlömer, C. von Stechow, et al., Renewable Energy Sources and Climate Change Mitigation: Special Report of the Intergovernmental Panel on Climate Change, Cambridge University Press, 2011.

[3] IEA, World Total Final Consumption By Source, IEA, Paris, 1971-2019, https://www.iea.org/data-and-statistics/charts/world-total-final-consumption-by-source-1971-2019.

[4] J. Sierra, D. González-Marco, J. Sospedra, X. Gironella, C. Mösso, A. Sánchez-Arcilla, Wave energy resource assessment in Lanzarote (Spain), Renew. Energy 55 (2013) 480–489, http://dx.doi.org/10.1016/j.renene.2013.01.004.

[5] G. Iglesias, R. Carballo, Wave resource in El Hierro—An island towards energy self-sufficiency, Renew. Energy 36 (2) (2011) 689–698.

[6] SWAN Team, et al., SWAN Scientific and Technical Documentation, SWAN Cycle III Version 40.81, Delft University of Technology, 2010.

[7] M. Gonçalves, P. Martinho, C.G. Soares, Wave energy assessment based on a 33-year hindcast for the Canary Islands, Renew. Energy 152 (2020) 259–269.

[8] L. Rusu, C.G. Soares, Wave energy assessments in the Azores Islands, Renew. Energy 45 (2012) 183–196.

[9] M. Bernardino, L. Rusu, C.G. Soares, Evaluation of the wave energy resources in the Cape Verde Islands, Renew. Energy 101 (2017) 316–326.

[10] M. Veigas, G. Iglesias, Wave and offshore wind potential for the island of Tenerife, Energy Convers. Manage. 76 (2013) 738–745.

[11] Red Eléctrica de España, work begins on the Salto de Chira, the first major energy storage system in the Canary Islands, 2022, URL https://www.ree.es/en/press-office/news/press-release/2022/02/work-begins-salto-de-chira-first-major-energy-storage-system-canary-islands.

[12] Y. Qiblawey, A. Alassi, M.Z. ul Abideen, S. Bañales, Techno-economic assessment of increasing the renewable energy supply in the Canary Islands: The case of Tenerife and Gran Canaria, Energy Policy 162 (2022) 112791.

[13] P.A. Bonar, I.G. Bryden, A.G. Borthwick, Social and ecological impacts of marine energy development, Renew. Sustain. Energy Rev. 47 (2015) 486–495.

[14] S. Astariz, C. Perez-Collazo, J. Abanades, G. Iglesias, Towards the optimal design of a co-located wind-wave farm, Energy 84 (2015) 15–24.
[15] S. Astariz, C. Perez-Collazo, J. Abanades, G. Iglesias, Co-located wind-wave farm synergies (operation & maintenance): A case study, Energy Convers. Manage. 91 (2015) 63–75.
[16] A. Saenz-Aguirre, J. Saenz, A. Ulazia, G. Ibarra-Berastegui, Optimal strategies of deployment of far offshore co-located wind-wave energy farms, Energy Convers. Manage. 251 (2022) 114914.
[17] E.D. Stoutenburg, N. Jenkins, M.Z. Jacobson, Power output variations of co-located offshore wind turbines and wave energy converters in California, Renew. Energy 35 (12) (2010) 2781–2791.
[18] S. Astariz, G. Iglesias, Selecting optimum locations for co-located wave and wind energy farms, Part I: The co-location feasibility index, Energy Convers. Manag. 122 (2016) 589–598.
[19] E. Gaughan, B. Fitzgerald, An assessment of the potential for co-located offshore wind and wave farms in Ireland, Energy 200 (2020) 117526.
[20] S. Rasool, K.M. Muttaqi, D. Sutanto, M. Hemer, Quantifying the reduction in power variability of co-located offshore wind-wave farms, Renew. Energy 185 (2022) 1018–1033.
[21] S.C. James, Y. Zhang, F. O'Donncha, A machine learning framework to forecast wave conditions, Coast. Eng. 137 (2018) 1–10.
[22] H. J., H. Smith, P. Challenor, Understanding uncertainty in a SWAN wave model using a Bayesian emulator, in: Proceedings: European Wave and Tidal Energy Conference, Plymouth, 2021.
[23] N. Booij, R.C. Ris, L.H. Holthuijsen, A third-generation wave model for coastal regions: 1. Model description and validation, J. Geophys. Res.: Oceans 104 (C4) (1999) 7649–7666.
[24] H. Hersbach, B. Bell, P. Berrisford, S. Hirahara, A. Horányi, J. Muñoz-Sabater, J. Nicolas, C. Peubey, R. Radu, D. Schepers, et al., The ERA5 global reanalysis, Q. J. R. Meteorol. Soc. 146 (730) (2020) 1999–2049.
[25] D. Christie, S.P. Neill, 8.09 - Measuring and observing the ocean renewable energy resource, in: T.M. Letcher (Ed.), Comprehensive Renewable Energy, second ed., Elsevier, Oxford, 2022, pp. 149–175, http://dx.doi.org/10.1016/B978-0-12-819727-1.00083-2, URL https://www.sciencedirect.com/science/article/pii/B9780128197271000832.
[26] G.J. Komen, L. Cavaleri, M. Donelan, K. Hasselmann, S. Hasselmann, P.A.E.M. Janssen, Dynamics and Modelling of Ocean Waves, Cambridge University Press, 1994, http://dx.doi.org/10.1017/CBO9780511628955.
[27] The Wamdi Group, The WAM model—A third generation ocean wave prediction model, J. Phys. Oceanogr. 18 (12) (1988) 1775–1810.
[28] B. Liang, H. Gao, Z. Shao, Characteristics of global waves based on the third-generation wave model SWAN, Mar. Struct. 64 (2019) 35–53.
[29] EMODnet Bathymetry Consortium, EMODnet digital bathymetry (DTM), 2020, http://dx.doi.org/10.12770/bb6a87dd-e579-4036-abe1-e649cea9881a.
[30] G.D. Egbert, S.Y. Erofeeva, Efficient inverse modeling of barotropic ocean tides, J. Atmos. Ocean. Technol. 19 (2) (2002) 183–204.
[31] L.P.S. Erofeeva, S.L. Howard, Tide model driver (TMD) version 2.5, 2020, https://www.github.com/EarthAndSpaceResearch/TMD_Matlab_Toolbox_v2.5.
[32] S.P. Neill, M.R. Hashemi, Wave power variability over the Northwest European shelf seas, Appl. Energy 106 (2013) 31–46.
[33] User manual SWAN cycle III version 41.41, 1993-2022.
[34] D. Lande-Sudall, T. Stallard, P. Stansby, Co-located deployment of offshore wind turbines with tidal stream turbine arrays for improved cost of electricity generation, Renew. Sustain. Energy Rev. 104 (2019) 492–503.
[35] A.M. Cornett, A global wave energy resource assessment, in: The Eighteenth International Offshore and Polar Engineering Conference, OnePetro, 2008.
[36] R.A. Gideon, E. Bou-Zeid, Collocating offshore wind and wave generators to reduce power output variability: A multi-site analysis, Renew. Energy 163 (2021) 1548–1559.